Advances in Science and Technology Research Journal

Advances in Science and Technology Research Journal, 2026, 20(7), 278–297
https://doi.org/10.12913/22998624/219823
ISSN 2299-8624, License CC-BY 4.0

Received: 2026.02.10
Accepted: 2026.05.15
Published: 2026.06.01

Heat transfer analysis of an intercooler in a natural gas compression station using copper oxide nanofluids

Edwin Calcina Ñaupa[1], Pascual Adriazola Corrales[1], José Canazas[1*], Christofer Alex Diaz Arapa[1]

[1] Universidad Nacional de San Agustín de Arequipa, Arequipa 04000, Perú
* Corresponding author's e-mail: jcanazas@unsa.edu.pe

ABSTRACT

Compact plate-fin intercoolers are widely used in natural gas compression stations; however, previous studies typically analyze isolated parameters, assume constant thermo-physical properties, or neglect the combined thermo-hydraulic impact of nanofluids under realistic operating conditions. This study presents a detailed numerical investigation of the thermo-hydraulic performance of a compact plate-fin intercooler evaluated for a natural gas compression station, explicitly addressing this gap through an integrated parametric framework. A model was implemented in Engineering Equation Solver using temperature-dependent thermo-physical properties for natural gas and the coolant, including copper oxide–water nanofluids. The effects of the gas Reynolds number (4000–12000), the imposed coolant-side temperature difference (8–12 °C), and the nanoparticle volume concentration (0–0.5%) were systematically evaluated in terms of overall heat transfer coefficient, required heat exchanger volume, and pressure drops on both sides. The results show that increasing the gas Reynolds number is the dominant enhancement mechanism, raising the overall heat transfer coefficient by approximately 35–40% and reducing the required volume by 30–45%, while increasing the gas-side pressure drop by 250–350%. However, the absolute magnitude of the gas-side pressure drop remains very small (approximately 2–18 Pa), representing a negligible fraction of the operating pressure of the compression system. Increasing the coolant temperature difference has a minor effect on the overall heat transfer coefficient (2–4%) but contributes to volume reduction with limited hydraulic impact. Nanofluids improve the overall heat transfer coefficient by 6–9% and reduce the required volume by up to 7–12%, although the coolant pressure drop increases due to higher effective viscosity. These findings provide a clearer thermo-hydraulic trade-off framework for compact intercooler design.

Keywords: intercooler, plate-fin heat exchanger, natural gas, nanofluid, heat transfer.

INTRODUCTION

Natural gas compression stations are essential components of transmission networks, ensuring the continuous transport of gas over long distances while maintaining adequate pressure levels [1]. The compression process leads to a substantial increase in gas temperature, which negatively impacts compressor efficiency, accelerates mechanical wear, and increases the thermal load on downstream equipment [2]. Therefore, intercoolers are integrated between compression stages to dissipate the excess heat generated during compression, reduce gas temperature, and improve the overall thermodynamic efficiency and operational reliability of the station [3]. Consequently, improving the heat transfer performance of intercoolers is of great interest from both an energy efficiency and economic perspective [4].

Conventional intercoolers operating in industry typically use water or water-based mixtures as cooling media [5]. While these fluids offer favorable availability and handling characteristics, their relatively low thermal conductivity imposes inherent limitations on improving heat transfer, especially with high mass flow rates and compact design constraints [6]. With the increasing demand for higher compression ratios, smaller

equipment sizes, and lower energy consumption, conventional heat transfer techniques are often insufficient to meet modern performance requirements. This has motivated the exploration of advanced cooling strategies capable of enhancing heat transfer without substantially modifying existing intercooler configurations [7].

Nanofluids, defined as suspensions of nanoscale solid particles dispersed in a base fluid, have become a promising approach for improving heat transfer in thermal systems [8][9]. Among various nanoparticulate materials, copper oxide (CuO) has attracted considerable attention due to its relatively high thermal conductivity, chemical stability, and compatibility with water-based coolants [10]. Numerous experimental and numerical studies have demonstrated that CuO nanofluids can significantly improve convective heat transfer coefficients compared to the base fluid [11], even with low particle volume fractions [12]. While the addition of nanoparticles can increase fluid viscosity and pressure drop, CuO nanofluids are typically characterized by a favorable ratio of thermal enhancement to hydraulic head loss, making them attractive for industrial heat exchanger applications [13].

Intercoolers in natural gas compression stations are commonly implemented as air-cooled, forced-ventilated finned-tube heat exchangers, especially in onshore pipeline applications where water availability is limited [14]. In installations where liquid cooling is feasible, shell-and-tube heat exchangers are also employed due to their mechanical robustness, ability to withstand high pressures, and ease of maintenance [15]. Although compact heat exchanger configurations offer higher surface area density, their application in high-pressure gas services can be limited by susceptibility to fouling, structural integrity, and maintenance requirements. The thermo-hydraulic performance of intercoolers is strongly influenced by the flow regime, the heat exchanger configuration, and the thermo-physical properties of the coolant. Therefore, the integration of CuO-based nanofluids requires a detailed evaluation of both the heat transfer improvement and the pressure drop penalties under realistic operating conditions.

Recent research has explored improved intercooler designs using nanofluids and advanced heat exchanger configurations for compressible gases. Several studies summarize how nanofluids enhance intercooler performance in gas turbine cycles, demonstrating improved heat transfer compared to conventional coolants. Zhao et al. [6] investigated the use of water-based nanofluids as coolants in an intercooler for a marine gas turbine intercooler cycle. The results showed that the nanofluids significantly improved heat transfer while reducing the required pumping power compared to conventional coolants. Almurtaji et al. [16] studied the application of water nanofluids and MWCNTs to improve the intercooler performance of a marine gas turbine. They showed a marked improvement in heat transfer and intercooler efficiency compared to conventional coolants. Mezrakchi [17] investigated the thermo-hydraulic performance of several hybrid nanofluids flowing through a tubular heat exchanger with different inlet velocities and Reynolds numbers. The results indicated that the CuO-ZnO-water hybrid nanofluid provided the greatest improvement in heat transfer, achieving a greater temperature reduction and Nusselt number, with a reduced friction factor compared to other nanofluids and the base fluid. Chintala et al. [18] experimentally evaluated the use of Al_2O_3-water nanofluids to improve heat transfer in the intercooler of a two-stage air compressor. They found that increasing the nanoparticle concentration significantly improved the intercooler's effectiveness and efficiency, with a maximum efficiency gain of approximately 6.1% at a volume concentration of 1%. Canazas and Kamyshnikov [19] numerically studied the thermal and hydraulic performance of a mining hydraulic shovel radiator using Al_2O_3-ethylene glycol nanofluids at different volume concentrations. The results indicated that nanofluids can improve heat transfer and reduce pressure drop under suitable thermal and flow conditions, highlighting the importance of optimizing operating parameters. Sahin and Ozturk [20] numerically analyzed heat transfer in a tubular heat exchanger using water and Al_2O_3- and SO_2-based nanofluids as coolants, with biogas as the hot fluid. It was observed that increasing the nanofluid concentration and Reynolds number led to a clear improvement in the heat transfer rate, with greater cooling observed near the tube bundles. Overall, these studies demonstrate the great potential of nanofluids to improve the performance of heat exchangers and intercoolers. However, they also highlight the need for further research that systematically links nanofluid properties, flow conditions, and heat exchanger configuration with practical applications of intercoolers for compressible gas systems.

Despite the extensive body of literature on compact heat exchangers and nanofluid applications, important limitations remain in the context of natural gas compression systems. Most previous studies focus either on conventional coolants, simplified geometries, or constant thermo-physical properties, and frequently analyze thermal or hydraulic performance separately rather than through an integrated thermo-hydraulic framework. Furthermore, the combined influence of gas-side flow intensity, imposed coolant temperature difference, and CuO–water nanofluid concentration has not been systematically evaluated for compact plate-fin intercoolers operating under realistic natural gas compression conditions. Consequently, a clear understanding of the thermo-hydraulic trade-offs governing exchanger sizing and pressure losses in such systems is still lacking. To address this gap, the present study develops a detailed numerical model incorporating temperature-dependent thermo-physical properties for both methane and CuO–water nanofluids and performs a structured parametric analysis covering practical operating ranges of Reynolds number, coolant temperature difference, and nanoparticle concentration. By simultaneously quantifying effects on overall heat transfer coefficient, required exchanger volume, and pressure drops on both sides, this work provides an integrated design-oriented assessment that advances the understanding of compact intercooler optimization for natural gas compression applications.

METHODOLOGY

Compression station description

In this study, a generic conventional compression station is considered, consisting of a compressor, two scrubbers, a contactor, and an intercooler, as shown in Figure 1. The performance of each component, and consequently the overall performance of the station, will not be analyzed in this work. However, some operational parameters of the system are considered as variables for the intercooler analysis.

After entering the station, the natural gas is directed to the suction scrubber, where it is separated from the liquids and condensate, each of which is sent to a different destination. The condensate is collected and pumped to the main gas outlet line, while the liquids are collected from each scrubber and sent to the combustion area for burial. Depending on the required pressure, the gas is compressed by a single- or multi-stage compressor after exiting the suction scrubber and being separated into compression trains via an inlet header. The gas must be cooled by an intercooler to reach the appropriate temperature, as compression raises its temperature. It's important to note that condensation occurs due to the compression and cooling of the gas. Installing a discharge scrubber is crucial to separate the liquids and send them to the equipment, since all vapors are converted into liquids through gas compression and cooling. The gas enters the contactor, a gas dehydrator, after being compressed to the required pressure. There, it is dehydrated before being sent to subsequent cooling facilities.

As mentioned previously, operational parameters are considered, which will be obtained from previous research considering the station's effective operation. The station's inlet and outlet pressures vary according to the station's operating conditions; however, in this case, an inlet pressure of 2500 kPa is considered, and a variable compression ratio, ranging from 2 to 3 [21], can be used. Furthermore, to simplify the model, a negligible pressure drop was assumed in the scrubbers, with a significant loss only in the intercoolers, where the flow presents greater resistance due to the internal configuration.

For this study, a compression ratio of 3 is considered. Additionally, a fixed mass flow rate of 120 kg/s is assumed [22, 23]. Assuming a compressor inlet temperature of 300 K, the natural gas inlet temperature to the intercooler can be determined, as shown in Equation 1 obtaining an inlet intercooler temperature from the gas side of 399 K, considering the compression ratio, an isentropic compressor efficiency of 90%, and the ratio of specific heats of the natural gas. It is then assumed that the natural gas outlet temperature from the intercooler should be the same as the inlet temperature of 300 K. The coolant inlet temperature is 293 K. For comparison purposes, the inlet pressure is arbitrary, since the parameter of interest is the pressure drop. Furthermore, the refrigerant mass flow rate is not arbitrarily imposed, but is calculated using the energy balance between the gas side and the refrigerant side (Equation 7).

$$T_2 = T_1 + \frac{T_1}{\eta_c}\left[r_c^{\frac{(\gamma_a-1)}{\gamma_a}} - 1\right] \tag{1}$$

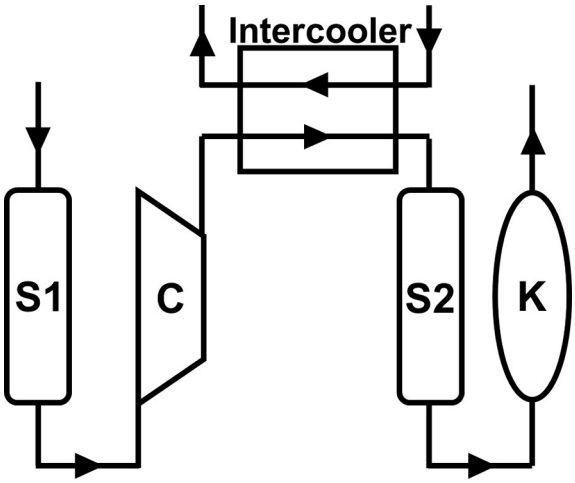

Figure 1. Layout of the natural gas compression station. S refers to the scrubbers, C refers to the compressor, and K refers to the contactor

Where the compression ratio is:

$$r_c = \frac{P_2}{P_1} \tag{2}$$

Intercooler description and mathematical model

The intercooler designed for cooling natural gas is considered a compact heat exchanger. In recent decades, this type of equipment has undergone extensive development, primarily through the optimization of fin geometry and dimensions, with the aim of improving thermal performance [24]. In this work, a plate-fin configuration is adopted for both the natural gas and coolant sides, using identical geometric dimensions on both sides of the exchanger. This type of configuration has been widely implemented in sectors such as the oil and gas industry, chemical processing, power generation, and heavy mobile machinery [19, 25]. The analyzed geometry is shown schematically in Figure 2, while its characteristic dimensions are summarized in Table 1. These dimensions were selected based on experimental data reported in real-world gas turbine applications [26]. The mathematical analysis both for the intercooler and working fluids of the present study is carried out in the software Engineering Equation Solver.

The following assumptions are made for the analysis: (i) the intercooler operates under steady-state conditions; (ii) the fins are assumed to have uniform thickness and negligible thermal resistance; (iii) all components of the heat exchanger are made of the same material, aluminum; and (iv) fouling and corrosion effects are not considered. To evaluate the intercooler's thermal performance, it is necessary to determine a series of characteristic geometric parameters on the gas and coolant sides. The expressions used to calculate these parameters are presented in Table 2, according to the methodology proposed by Kays and London [26]. It is important to mention that in Equation 5, subscripts 1 and 2 refer to the gas side and the coolant side, respectively. That is, the plate spacing for each side of the fluid.

Table 1. Structural dimensions of the plate-fin heat exchanger, the symbols are shown in Figure 2

Parameter	Symbol	Both sides
Fin configuration	-	Plain
Fin thickness (mm)	t	0.25
Fin height (mm)	h	10.05
Plate spacing (mm)	b	10.3
Fin spacing (mm)	s	3.8
Plate thickness (mm)	a	0.8

In the heat transfer analysis, the temperature, pressure, and mass flow rates of the gas at the intercooler inlet are considered fixed. Similarly, for the coolant, a constant ambient inlet temperature, a pumping pressure sufficient to ensure flow through the exchanger, and a fixed mass flow rate are assumed. Since the intercooler belongs to the category of compact heat exchangers, the energy balance equation shown in Equation 7 is used to relate the heat exchange between both fluids, allowing the required mass flow rate of the coolant to be determined [19].

$$Q = \dot{m}_c c_c \left(T_{c,o} - T_{c,i}\right) = \\ = \dot{m}_g c_g (T_{g,i} - T_{g.o}) \tag{7}$$

The mass velocity and Reynolds number on both sides of the heat exchanger are calculated using Equations 8 and 9, respectively. In this analysis, the mass velocity is defined as a function of the fin spacing. It is important to note that calculating this velocity requires knowing the frontal flow area on both sides, a parameter that is initially unknown because sizing the heat exchanger is one of the objectives of this study. For this reason, the procedure adopted is iterative and leads to multiple possible solutions,

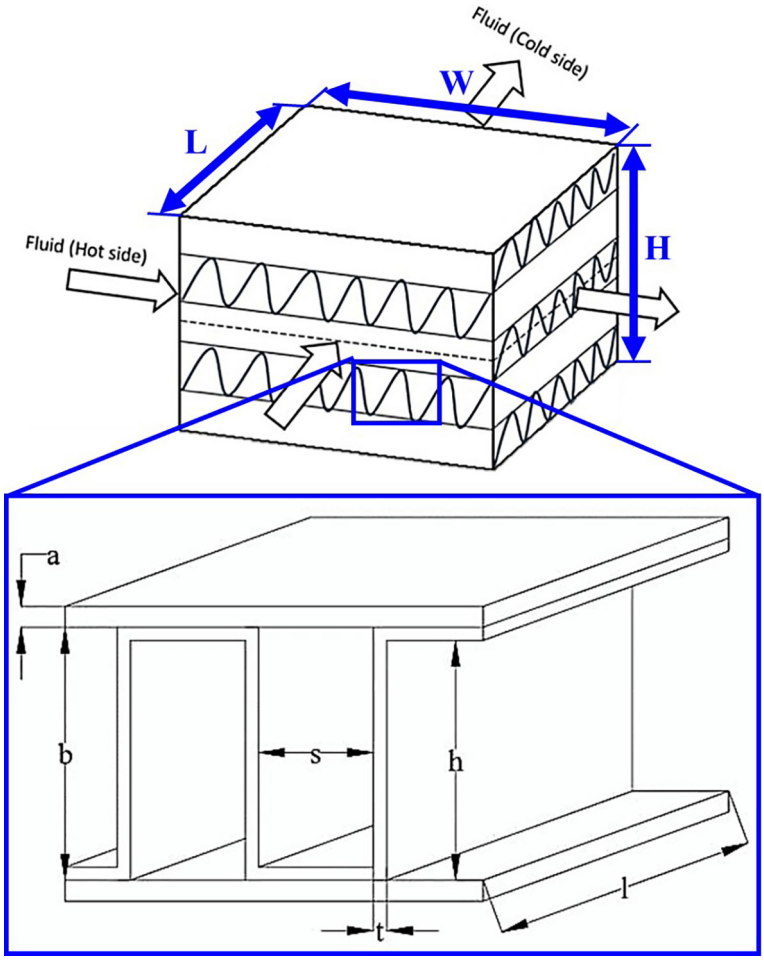

Figure 2. Schematic geometries of the plate-fin heat exchanger configuration (from [19, 27]). The top shows a schematic isometric drawing of the intercooler, and the bottom shows a detail of the heights

evaluating different geometric combinations to analyze their influence on heat transfer and pressure drop. This procedure is detailed later, after obtaining the overall heat transfer coefficient.

$$G = \frac{\dot{m}}{A_{fr} \times \sigma} \tag{8}$$

$$Re = \frac{D_h G}{\mu} \tag{9}$$

Where:

$$A_{fr,g} = LH \tag{10}$$

$$A_{fr,c} = WH \tag{11}$$

To determine the final dimensions of the intercooler, it is necessary to calculate the overall heat transfer coefficient on the gas side, which depends on the convective coefficients and the surface efficiency of the fins on both sides of the exchanger. First, the friction factor for turbulent flow proposed by Vajjha et al. [28], shown in Equation 12, is considered. From this factor, Gnielinski [29] developed the correlation for the Nusselt number in turbulent flow, presented in Equation 13. In Equation 12, the subscripts nf and bf stand for nanofluid and base fluid respectively.

$$f_c = 0.3164 Re_c^{-0.25} \left(\frac{\rho_{nf}}{\rho_{bf}}\right)^{0.797} \left(\frac{\mu_{nf}}{\mu_{bf}}\right)^{0.108} \tag{12}$$

$$Nu_c = \frac{\left(\frac{f_c}{8}\right)(Re_c - 1000)Pr_c}{1 + 12.7\sqrt{\frac{f_c}{8}}\left(Pr_c^{\frac{2}{3}} - 1\right)} \left[1 + \left(\frac{D_{h,c}}{L}\right)^{\frac{2}{3}}\right] \left(\frac{Pr_c}{Pr_w}\right)^{0.11} \tag{13}$$

Table 2. Equations of the geometry parameters for the analysis

Parameter	Formula	Equation
Hydraulic radius (m)	$r_h = \frac{D_h}{4} = \frac{2sh}{s+h}$	(3)
Total transfer area/volume between plates (m^2/m^3)	$\beta = \frac{2(h+s)}{b(s+t)}$	(4)
Tota transfer area/ total heat exchanger volume (m^2/m^3)	$\alpha = \frac{\beta b}{b_1 + b_2 + 2a}$	(5)
Free flow area/ frontal area	$\sigma = r_h \alpha$	(6)

Then, the heat transfer coefficient on the coolant side is shown in Equation 14.

$$h_c = \frac{Nu_c k_c}{D_{h,c}} \tag{14}$$

For the gas side, experimental data from Kays and London [26] for flat fin surfaces were used, which were adjusted using empirical correlations for the Colburn factor and the friction factor, valid for turbulent flow up to a Reynolds number of 12,000, as shown in Equations 15 and 16 [19].

$$j_g = -3.8 \cdot 10^{-8} Re_a + 0.00348 \tag{15}$$

$$f_g = 2.4 \cdot 10^{-11} Re_a^2 - 5.9 \cdot 10^{-7} Re_a + 0.0108 \tag{16}$$

From these correlations, the gas-side convective coefficient was determined, expressed in Equation 17.

$$h_g = \frac{j_g G_g c_g}{Pr_g^{2/3}} \tag{17}$$

The overall heat transfer coefficient is finally calculated using Equation 21, incorporating the effect of fin efficiency and surface effectiveness. In this analysis, the thermal resistance of the wall is neglected due to its small magnitude and the use of the same structural parameters on both sides of the heat exchanger.

$$m_f = \sqrt{\frac{2h_{fluid}}{k_{Al} t}} \tag{18}$$

$$\eta_f = \frac{tanh(m_f(h+t))}{m_f(h+t)} \tag{19}$$

$$\eta_o = 1 - \frac{A_f}{A_T}(1 - \eta_f) \tag{20}$$

$$\frac{1}{U} = \frac{1}{\eta_{o,g} h_g} + \frac{1}{\eta_{o,c} h_c} \tag{21}$$

Once the overall heat transfer coefficient is obtained, the ε–NTU method is used to determine the required heat transfer area. The heat exchanger effectiveness is calculated using Equation 22, while the NTU for a cross-flow heat exchanger with both fluids unmixed is obtained from Equation 23.

$$\epsilon = \frac{q}{q_{max}} = \frac{C_g |T_{g,in} - T_{g,out}|}{C_{min} |T_{g,in} - T_{c,in}|} = \frac{C_c |T_{c,in} - T_{c,out}|}{C_{min} |T_{g,in} - T_{c,in}|} \tag{22}$$

$$\epsilon = 1 - exp[\frac{exp(-NTU^{0.78} C) - 1}{NTU^{-0.22} C}] \tag{23}$$

From Equations 22 and 23, C_g and C_c represent the heat capacity rate on the gas and coolant sides, respectively, and are obtained through Equations 24 and 25. Additionally, Equation 26 shows the minimum heat capacity rate ratio; C_{min} refers to the lowest heat capacity rate between the two sides, and C_{max} to the highest.

$$C_g = \dot{m}_g c_g \tag{24}$$

$$C_c = \dot{m}_c c_c \tag{25}$$

$$C = \frac{C_{min}}{C_{max}} \tag{26}$$

Subsequently, the heat transfer area is determined using the relationship shown in Equation 27. This value is compared with the proposed initial area, defined as a function of the exchanger volume (Equations 28 and 29), which reinforces the iterative nature of the design process. Since the heat exchanger volume is obtained from three dimensions as shown in Equation 29, for the iterative process two of these three parameters are modified so that the heat transfer areas of Equations 27 and 28 are equivalent. In our specific case, the dimension H is the one that influences the frontal area of each side, so it remains constant,

and only the dimensions W and L are varied, for the coolant side and the gas side respectively.

$$A = \frac{C_{min} NTU}{U} \tag{27}$$

$$A = \alpha V \tag{28}$$

Where:

$$V = WLH \tag{29}$$

Finally, once the geometric dimensions of the intercooler are defined, the pressure drop on each side is calculated using the expression for single-phase flow presented in Equation 30, which allows the hydraulic performance of the system to be evaluated along with its thermal behavior.

$$\Delta P = \frac{f L_r G^2}{2 D_h \rho} \tag{30}$$

It is important to note that the pressure drop model employed in this study accounts primarily for distributed (frictional) losses within the heat exchanger channels, based on well-established correlations for compact plate-fin geometries. However, in practical engineering systems, additional pressure losses may arise due to flow distribution effects, including inlet and outlet headers, manifolds, and potential flow maldistribution among parallel channels. These effects are not explicitly included in the present model, as the analysis focuses on the intrinsic thermo-hydraulic behavior of the heat transfer core. In large-scale exchangers, particularly when the overall dimensions increase and multiple channels are supplied through common headers, such additional losses may become non-negligible and can contribute significantly to the total pressure drop. Therefore, the gas-side pressure drop values reported in this work should be interpreted as an estimation of the core (channel-level) frictional contribution, which may represent a lower bound of the total pressure drop in real installations. A more comprehensive evaluation including header design, flow distribution, and three-dimensional effects would be required for detailed industrial design and is recommended for future research.

Thermo-physical properties of the fluids

Correlations for the density, specific heat, dynamic viscosity, and thermal conductivity of the base fluid, natural gas, and nanofluids are necessary for the analysis. These correlations were established from the data by fitting curves within a suitable temperature range. In this study, methane (CH_4) is used as the representative component of natural gas in the simulation. Although natural gas is a mixture composed primarily of methane along with other hydrocarbons (e.g., ethane, propane) and inert gases (e.g., nitrogen, CO_2), methane typically constitutes between 85% and 95% of the mixture by volume. Since methane dominates the thermo-physical properties of natural gas, to simplify modeling and calculations it is considered an acceptable approximation to simulate the thermal and flow behavior of natural gas-based systems [30,31].

Therefore, Table 3 shows the thermophysical correlations for methane. The information was obtained from previous research, considered a natural gas database. In this case, only the density is shown to depend on static pressure; in other words, the specific volume of natural gas varies with this parameter. The other transport and caloric properties of methane exhibit minimal pressure dependence under typical (subcritical) conditions. Experimental data show that thermal conductivity and viscosity change by <3% at pressures up to 70 MPa [32, 33], while specific heat changes by <0.5% at pressures up to 33 MPa [34], which is consistent with ideal gas law.

According to the literature on heat exchanger workflow, there is no general agreement on which fluid is most appropriate; however, some details are taken into account depending on the application. For example, in various applications, a mixture of water and ethylene glycol is used due to environmental conditions, as the fluid has a higher boiling point and a lower freezing point. However, due to its abundance, this research will use water as the base fluid, since it has superior thermo-physical properties to ethylene glycol and its blends, and there is a larger body of research on nanoparticles suspended in this liquid. Table 4 illustrates these properties, and the coefficient of determination is close to 1. A series of data sources, considered databases for water [35–37], were used to obtain the property data, and a curve was fitted in relation to temperature, between 290 K and 310 K, the range in which the system will operate.

Although nanofluids have been extensively studied and subjected to numerous experimental tests, a completely detailed characterization of their properties from all possible perspectives

Table 3. Correlations of the thermo-physical properties of methane for 300 K ≤ T ≤ 500 K. And additionally, the density for 100 kPa ≤ P ≤ 600 kPa

Property	Correlation	Eq.
Density (kg/m³)	$\rho = \frac{P}{518.36T}$	(31)
Specific heat (J/kg-K)	$c = 3.85 \cdot 10^{-4}T^2 - 0.18T + 1025.73$	(32)
Thermal conductivity (W/m-K)	$k = 6.95 \cdot 10^{-5}T + 4.94 \cdot 10^{-3}$	(33)
Viscosity (Pa.s)	$\mu = -2.54 \cdot 10^{-11}T^2 - 6.12 \cdot 10^{-8}T + 2.49 \cdot 10^{-6}$	(34)

is still not available. This is due, among other factors, to variations in nanomaterial synthesis methods and the influence of different physicochemical parameters [38, 39]. However, it is possible to use previous studies to estimate these properties. In particular, the density and specific heat of nanofluids, for different temperatures and volume fractions, can be calculated using the empirical correlations presented in Equations 39 and 40, respectively [40, 41]. In the specific case of copper oxide nanoparticles, an approximate density of 6500 kg/m³ is considered, while their specific heat is estimated at 525 J/(kg·K) [42]. In Equations 39, 40, 41 and 42, the subscripts nf, np and bf stand for nanofluid, nanoparticle and base fluid respectively.

$$\rho_{nf} = \phi\rho_{np} + (1-\phi)\rho_{bf} \tag{39}$$

$$(\rho c)_{nf} = \phi(\rho c)_{np} + (1-\phi)(\rho c)_{bf} \tag{40}$$

According to the study carried out by Girhe et al [43], correlations were developed for the thermal conductivity and viscosity of copper oxide dispersed in water for a range of temperatures (290 K ≤ T ≤ 340 K) and concentrations (0.1% ≤ ϕ ≤ 0.5%) shown in Equations 41 and 42 respectively.

$$\frac{k_{nf}}{k_{bf}} = 1 + 0.008 (T-273)^{0.97}\phi^{0.79} \tag{41}$$

$$\frac{\mu_{nf}}{\mu_{bf}} = 1.02e^{\frac{-0.8}{T-273}+0.25\phi} \tag{42}$$

Figure 3 shows a flowchart of the entire numerical methodology adopted for the evaluation of heat transfer, pressure drop and intercooler sizing for the natural gas compression station.

It is important to note that although no direct experimental validation was performed within the scope of this study, the numerical model is constructed exclusively using well-established and experimentally validated correlations for compact plate-fin heat exchangers and turbulent internal flows. The heat transfer and friction factor correlations employed for both the gas and coolant sides have been extensively reported in the literature and are applicable within the Reynolds number ranges analyzed.

RESULTS

This section presents and analyzes the results obtained from the numerical model developed for the compact intercooler used in a natural gas compression station. The analysis focuses on the influence of three key parameters on the system's thermal and hydraulic performance: (i) the Reynolds number of the natural gas, (ii) the imposed temperature delta of the coolant in the intercooler, and (iii) the volumetric concentration of CuO nanoparticles in the coolant. For each case, the overall heat transfer coefficient, the required

Table 4. Correlations of the thermo-physical properties of water for 290 K ≤ T ≤ 320 K

Property	Correlation	Eq.
Density (kg/m³)	$\rho = -4.72 \cdot 10^{-3}T^2 + 2.56T + 653.58$	(35)
Specific heat (J/kg-K)	$c = -2.19 \cdot 10^{-2}T + 4189.6$	(36)
Thermal conductivity (W/m-K)	$k = -9.73 \cdot 10^{-6}T^2 + 7.49 \cdot 10^{-3}T - 0.77$	(37)
Viscosity (Pa.s)	$\mu = 3.48 \cdot 10^{-7}T^2 - 2.28 \cdot 10^{-4}T + 3.79 \cdot 10^{-2}$	(38)

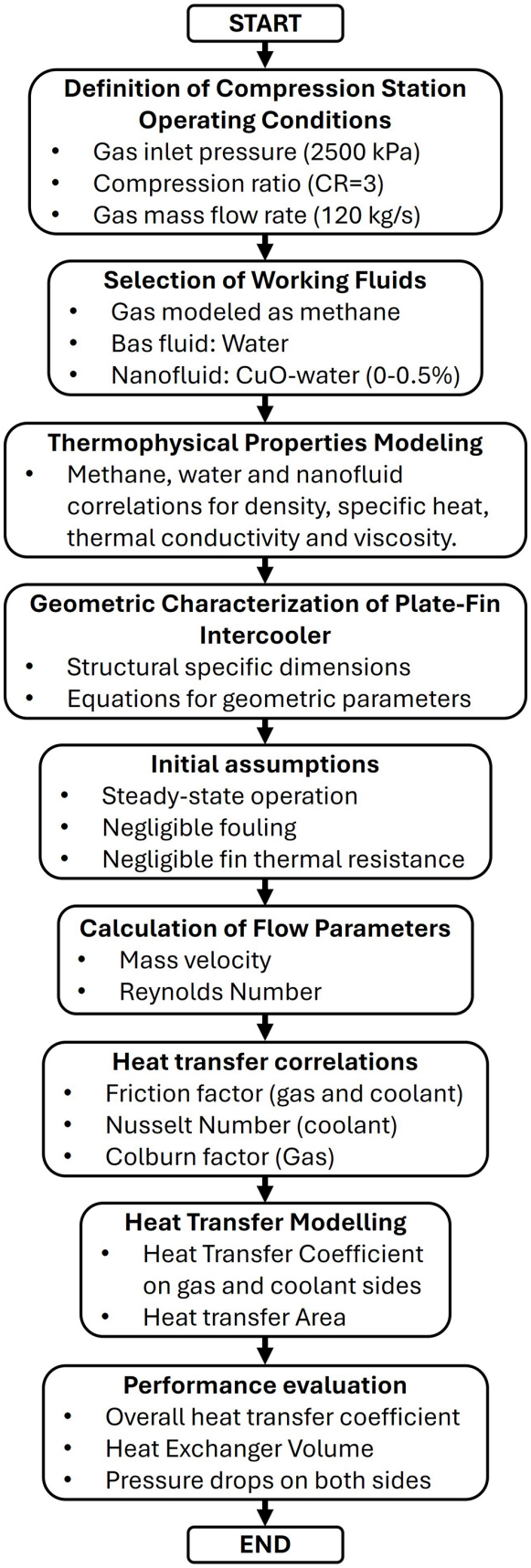

Figure 3. Flowchart of the methodology adopted for the thermo-hydraulic evaluation and sizing of the intercooler

exchanger volume, and the pressure drops on both sides are evaluated to identify dominant physical trends and relevant thermo-hydraulic trade-offs for real-world industrial applications.

Influence of the gas Reynolds number

This section systematically analyzes the influence of the Reynolds number of natural gas on the thermal and hydraulic behavior of the compact intercooler. The analysis is performed for gas Reynolds numbers between 4000 and 12000, keeping the coolant mass flow rate, the target temperature difference of the gas, and the heat exchanger geometry constant.

Figure 4 shows the variation of the overall heat transfer coefficient U as a function of the coolant Reynolds number for different gas Reynolds numbers. For a fixed coolant Reynolds number, increasing the gas Reynolds number produces a clear and sustained increase in U. For example, for an intermediate coolant Reynolds number, the overall heat transfer coefficient increases by approximately 35–40% when the gas Reynolds number is increased from 4000 to 12000. This increase is mainly associated with the intensification of the convective coefficient on the gas side, where thermal resistance is usually dominant in compact gas-liquid heat exchangers.

However, the increase in U is not linear across the entire gas Reynolds number range. From 4000 to 8000, the relative increase in U is on the order of 20–25%, while the additional increase from 8000 to 12000 is reduced to approximately 10–15%. This behavior indicates the emergence of diminishing returns, a phenomenon widely reported in the literature for compact heat exchangers with finned surfaces, where other thermal resistances – such as those on the coolant side and fin efficiency – begin to limit the overall improvement in heat exchange.

The influence of the gas Reynolds number on the heat exchanger sizing is shown in Figure 5, which presents the total required intercooler volume. Increasing the gas Reynolds number leads to a significant reduction in the volume needed to meet the imposed thermal load. In quantitative terms, the percentage reduction in heat exchanger volume when increasing the gas Reynolds number from 4000 to 6000 and to 12000 was determined to be 30% and 55%, respectively. This reduction is a direct result of the increased overall heat transfer coefficient, which allows the same thermal effectiveness to be achieved with a smaller heat transfer area.

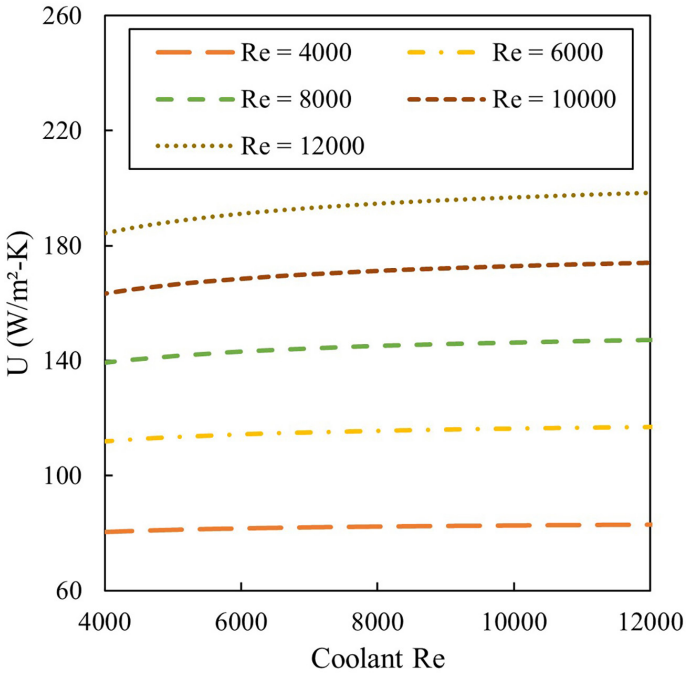

Figure 4. Overall heat transfer coefficient evaluated with different gas Reynolds numbers for a range of 4000 to 12000 of the coolant Reynolds number

Similar to what was observed for the overall coefficient, the volume reduction exhibits an asymptotic trend. Most of the volume reduction is achieved by increasing the gas Reynolds number from low to intermediate values, while at high gas Reynolds numbers, the further reduction is more limited. From a practical standpoint, this result is highly relevant, as it suggests that operating at excessively high gas Reynolds numbers may not be efficient when hydraulic penalties are also considered.

The effect of the gas Reynolds number on the coolant-side pressure drop is shown in Figure 6. The results indicate that the coolant pressure drop is relatively insensitive to variations in the gas Reynolds number. Across the entire analyzed range, the maximum increase in the coolant pressure drop is less than 5–8% when the gas Reynolds number is increased from 4000 to 12000. This behavior is explained by the fact that the hydrodynamic conditions of the coolant remain constant and that the thermal interaction with the gas only marginally modifies the average properties of the coolant fluid. Consequently, from the point of view of coolant pumping, the increase in gas Reynolds number does not introduce a significant penalty.

Conversely, Figure 7 shows that the pressure drop on the gas side increases with the gas Reynolds number. When the gas Reynolds number rises from 4000 to 12000, the gas pressure drop increases proportionally; however, its absolute magnitude remains low, with a maximum value of approximately 18 Pa. Compared with the gas inlet pressure of 2500 kPa prior to compression, this variation can be considered negligible from a practical and operational standpoint. Therefore, although the relative increase is noticeable from a fluid-dynamic perspective, its impact on compressor power requirements is minimal under the studied conditions.

The relatively small gas-side pressure drop obtained in the present study is mainly related to the geometric characteristics of the analyzed heat exchanger configuration. In the adopted design methodology, the exchanger height (H) is varied while maintaining the required heat transfer area according to Equations 27 and 28. As a consequence, when H decreases, the exchanger length (L) increases to preserve the overall heat transfer surface. The obtained gas-side pressure drops remain on the order of only a few Pascals (approximately 2–18 Pa), which represents a negligible fraction of the compressor operating pressure level (MPa order).

However, the gas flow direction corresponds to the exchanger width (W), which remains smaller than 1 m for all evaluated configurations.

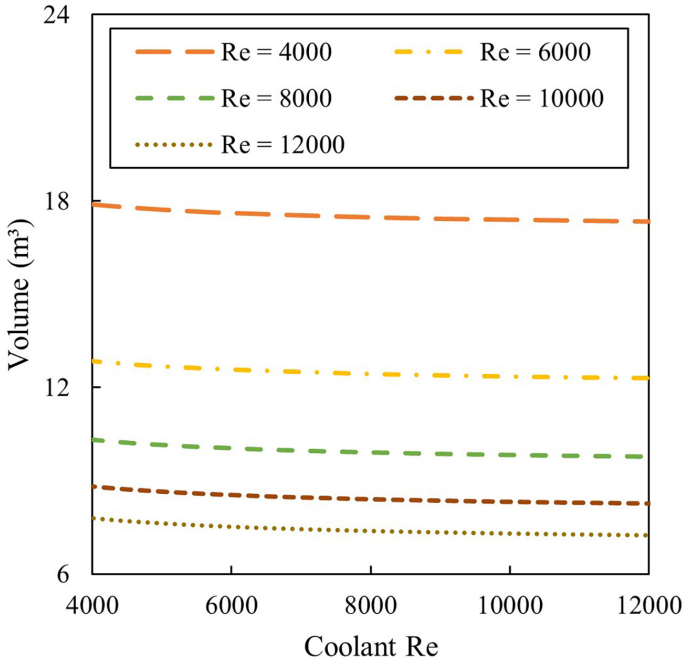

Figure 5. Intercooler volume evaluated with different gas Reynolds numbers for a range of 4000 to 12000 of the coolant Reynolds number

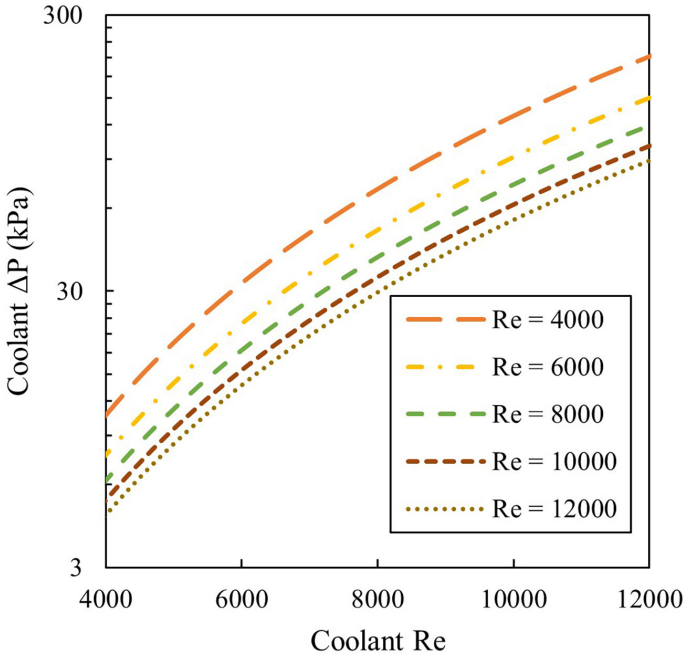

Figure 6. Pressure drop on the coolant side evaluated with different gas Reynolds numbers for a range of 4000 to 12000 of the coolant Reynolds number

Therefore, the actual gas flow path length is relatively short and varies only slightly between cases. Because frictional pressure losses are directly related to the flow path length, the resulting gas-side pressure drop remains small even at higher Reynolds numbers. Furthermore, as the exchanger volume increases, the effective flow area also increases, which reduces the gas velocity and consequently decreases the frictional pressure losses. This explains the decrease in pressure drop shown in Figure 7 with the increase in heat exchanger volume presented in Figure 5.

Taken together, the results in this section confirm that the gas Reynolds number

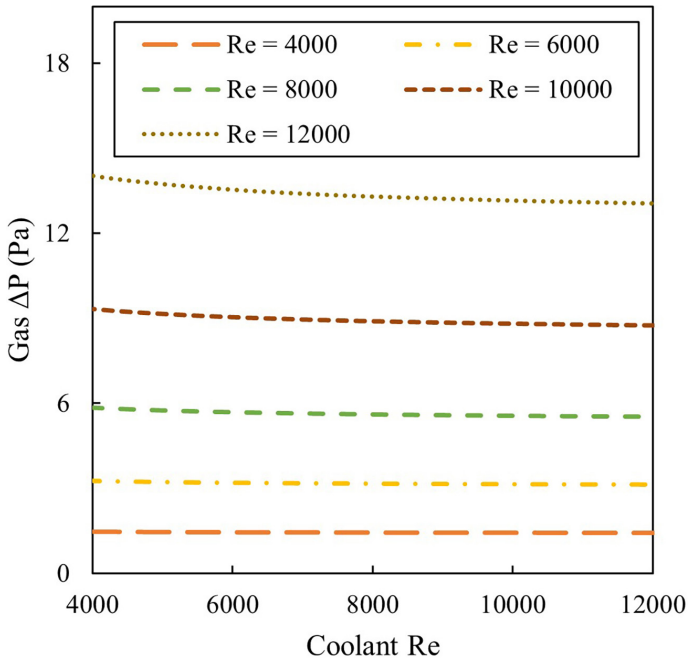

Figure 7. Pressure drop on the gas side evaluated with different gas Reynolds numbers for a range of 4000 to 12000 of the coolant Reynolds number

significantly influences the thermal performance of the intercooler, primarily through the enhancement of the overall heat transfer coefficient and the associated reduction in exchanger volume. This behavior is consistent with classical turbulent convection trends reported for compact plate-fin heat exchangers, where increasing Reynolds number intensifies convective transport while increasing frictional losses. Similar tendencies have been documented in previous studies; however, the present analysis extends those findings by quantifying the simultaneous impact on exchanger sizing under realistic natural gas compression conditions, thereby providing a more design-oriented thermo-hydraulic assessment. Although higher gas Reynolds numbers increase the gas-side pressure drop, this effect remains negligible in absolute terms when compared with the operating pressure level of the system. Consequently, within the evaluated range, the thermo-hydraulic trade-off is predominantly governed by heat transfer enhancement rather than gas-side hydraulic penalties. In the subsequent sections, this analysis is complemented by evaluating the influence of the imposed temperature difference and the nanofluid concentration in order to identify configurations that improve thermal performance without introducing significant hydraulic drawbacks.

Influence of temperature deltab on the coolant side

This section analyzes the effect of the imposed temperature difference (ΔT) between the inlet and outlet on the coolant side on the thermal and hydraulic performance of the intercooler. This delta value is imposed on heat exchangers due to thermal fluctuations on the coolant side, which can be managed with temperature sensing. The analysis is performed for ΔT values of 8, 10, and 12 °C, keeping the gas Reynolds number constant at 8000, a value representative of a previously analyzed intermediate operating condition.

Figure 8 shows the variation of the overall heat transfer coefficient (U) as a function of the coolant Reynolds number for the different ΔT values. It can be observed that, in all cases, U increases with increasing coolant Reynolds number, which is consistent with the expected behavior in turbulent internal flow, where increased velocity increases the convective coefficient and reduces the thermal resistance associated with the boundary film. However, when comparing the three ΔT values, it is clear that the temperature difference has a secondary influence on U, with relatively small differences between the curves. In quantitative terms, the increase in ΔT from 8 to 12 °C produces an increase in U of approximately 2–4%, depending on the Reynolds number of the

coolant. This result indicates that the overall coefficient is primarily controlled by the convective regime (Reynolds) and by the average thermophysical properties, while the temperature difference does not significantly alter the heat transfer mechanisms within the analyzed range.

This behavior can be explained by the classical formulation of the overall heat transfer coefficient (ΔT), where U depends on the sum of the thermal resistances in series (gas side, metal wall, and coolant side), as well as the surface efficiency associated with the fins. In this context, ΔT does not directly modify the convection mechanism but rather acts primarily on the overall thermal driving force. Because the Nusselt correlations used depend mainly on Re and Pr, and the temperature range considered does not drastically alter the properties of the gas or the coolant, the variation of U remains limited. This is consistent with trends reported in compact gas-liquid heat exchangers, where moderate temperature changes more significantly affect the heat capacity and the mean temperature difference than the convective heat transfer coefficient.

Despite the limited influence of ΔT on the overall heat transfer coefficient, its effect on intercooler sizing is clearly reflected in Figure 9. The results show that, for a fixed gas Reynolds number of 8000, the required heat exchanger volume increases as the imposed coolant-side temperature difference (ΔT) increases. For all coolant Reynolds numbers, the highest volume corresponds to ΔT = 12 °C, while the lowest is obtained for ΔT = 8 °C. Additionally, increasing the coolant Reynolds number leads to a progressive reduction in volume for all ΔT values. These trends indicate that, under the modeled conditions, the exchanger sizing is more strongly influenced by the coolant flow rate than by the imposed temperature difference, and that larger ΔT values do not lead to a reduction in the required volume in the present configuration.

From an industrial design perspective, this trend is relevant because it suggests that operational control of the temperature difference (for example, by regulating the coolant flow rate or inlet temperature) can be used as a tool for intercooler compaction without significantly increasing pressure losses. However, it is important to note that an excessive increase in the temperature difference could affect downstream system performance (for example, thermal conditions in the subsequent compression stage), so its optimization must consider thermodynamic constraints of the overall process.

The influence of ΔT on hydraulic performance is presented in Figure 10. The results indicate that the coolant-side pressure drop increases both with

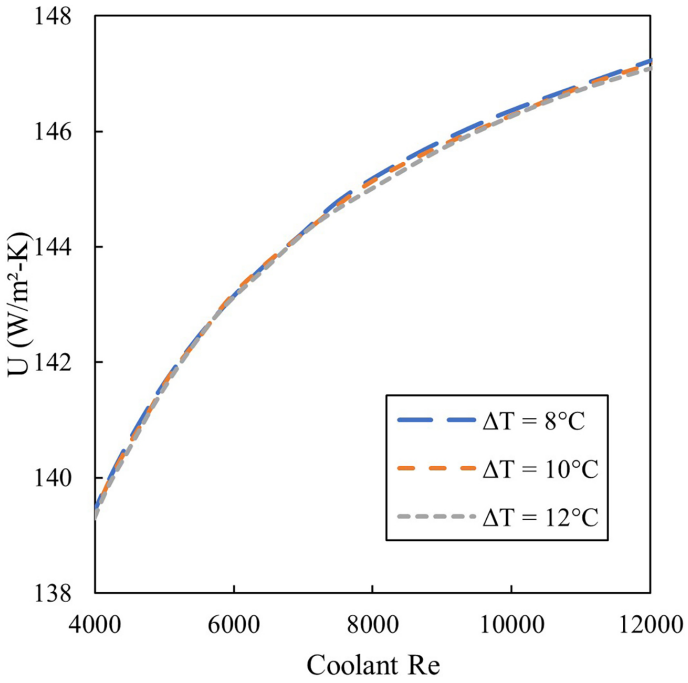

Figure 8. Overall heat transfer coefficient evaluated with different temperature deltas on the coolant side for Re_g = 8000, for a range of 4000 to 12000 of the coolant Reynolds number

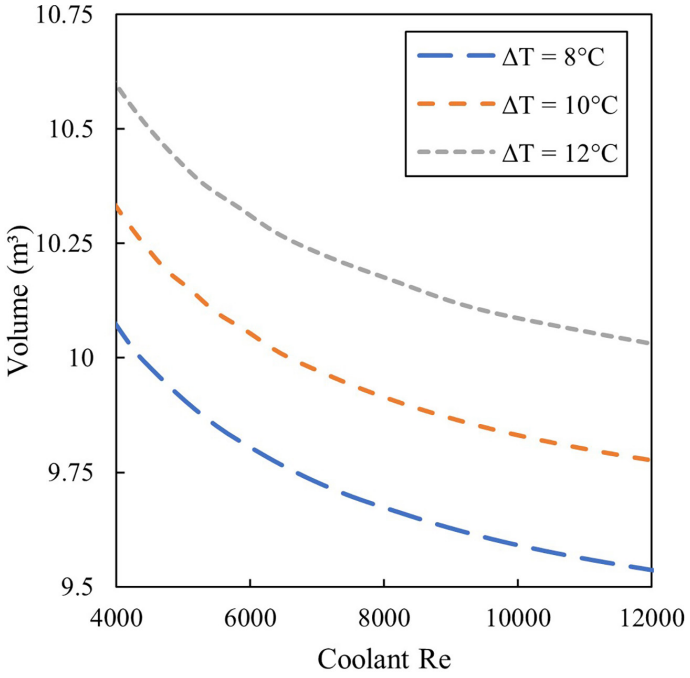

Figure 9. Intercooler volume evaluated with different coolant side temperature deltas for Re_g = 8000, for a range of 4000 to 12000 of the coolant Reynolds number

coolant Reynolds number and with increasing ΔT. For a given Reynolds number, the highest pressure losses correspond to ΔT = 12 °C, whereas the lowest values are observed for ΔT = 8 °C. This behavior suggests that, within the evaluated temperature range, the increase in average coolant temperature does not produce a sufficient viscosity reduction to offset the higher flow-related hydraulic effects. Consequently, in contrast to the initial assumption, higher ΔT values are associated with slightly higher pressure drops under the simulated conditions.

On the gas side (Figure 11), the pressure drop shows a weak dependence on the temperature difference, exhibiting variations of less than 5% across the entire analyzed range. This indicates that, for the fixed gas Reynolds number of 8000, the gas hydrodynamics are dominated by the mass velocity and the heat exchanger geometry, while the variations in properties with temperature are not large enough to significantly modify the pressure losses. Consequently, the temperature difference can be considered an adjustment parameter with low hydraulic impact on the gas side, which is advantageous in compression stations where the most critical energy penalty is usually associated with the compressor power.

Collectively, the results of this section demonstrate that increasing ΔT is an effective strategy for reducing intercooler size and improving system compactness, while maintaining a nearly constant overall heat transfer coefficient and without introducing significant hydraulic penalties. This behavior is consistent with previous analyses of compact intercoolers, where the imposed temperature difference primarily influences exchanger sizing through the available thermal driving force rather than substantially modifying local convective heat transfer coefficients. In contrast to studies that focus mainly on thermal performance, the present work additionally evaluates the associated hydraulic response, enabling a more comprehensive thermo-hydraulic assessment. Within the analyzed range, these findings suggest that intercooler optimization may benefit more from adjusting the temperature difference as an operational design variable than from attempting to enhance U through temperature variations alone.

Influence of nanofluid concentration

The influence of the volumetric concentration of CuO nanoparticles in the coolant is analyzed in this section considering values of ϕ = 0, 0.1, 0.3, and 0.5%, while keeping the gas Reynolds number constant at 8000. This analysis allows for the evaluation of the real potential of nanofluids to improve the thermo-hydraulic

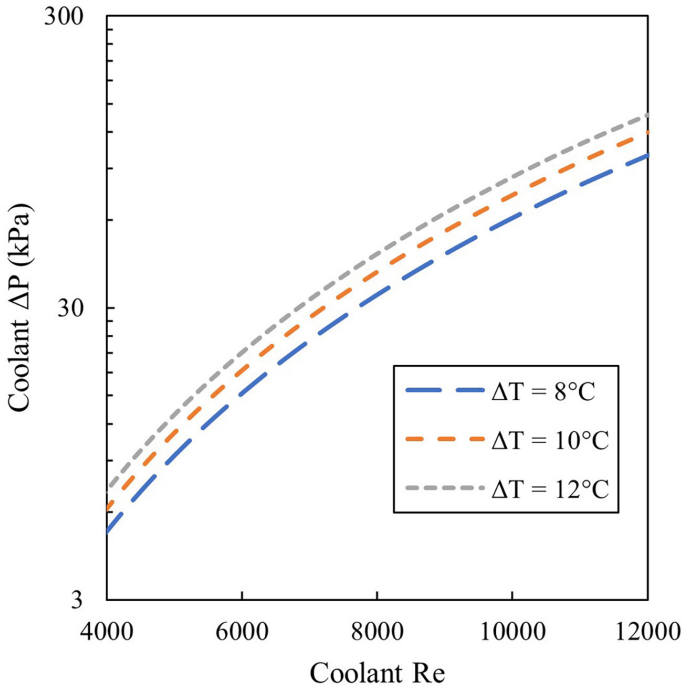

Figure 10. Pressure drop on the coolant side evaluated with different temperature deltas on the coolant side for Re_g = 8000, for a range of 4000 to 12000 of the coolant Reynolds number

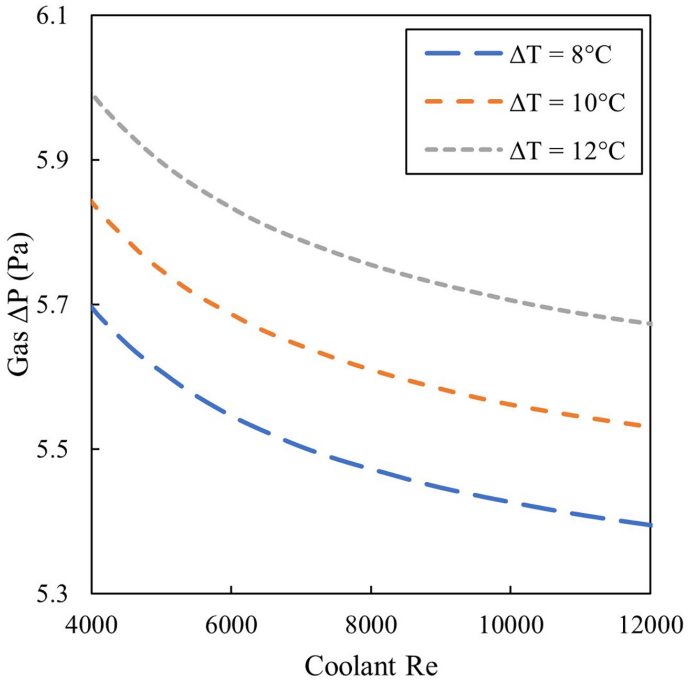

Figure 11. Pressure drop on the gas side evaluated with different temperature deltas on the coolant side for Re_g = 8000, for a range of 4000 to 12000 of the coolant Reynolds number

performance of the intercooler under representative operating conditions.

Figure 12 shows the overall heat transfer coefficient U as a function of the coolant Reynolds number for the different concentrations. It can be observed that, for all concentrations, U increases with the coolant Reynolds number, confirming that the convective regime remains the dominant mechanism. However, as ϕ increases, a systematic shift towards higher U values is observed, demonstrating the positive effect of the nanofluid. Quantitatively, as the concentration increases

from $\phi = 0$ to $\phi = 0.5\%$, the overall coefficient increases by approximately 6% to 9%, depending on the coolant Reynolds number. This result is consistent with the improvement in the effective thermal conductivity of the coolant, which increases the convective coefficient on the liquid side and reduces the overall thermal resistance.

From a physical standpoint, the increase in U with concentration can be attributed to several mechanisms. First, the increased thermal conductivity of the nanofluid enhances energy transport by conduction in the thermal boundary layer. Second, some nanofluid models suggest additional effects associated with Brownian motion, microconvection, and alteration of the effective thermal gradient, which can contribute to intensifying energy exchange. However, in compact heat exchangers and under turbulent conditions, the dominant contribution is usually the modification of effective thermo-physical properties, especially k and Pr, which is consistent with the observed trends.

The impact of the thermal improvement on sizing is shown in Figure 13, which displays the required intercooler volume. A reduction in volume is observed as ϕ increases, which is consistent with the observed increase in U. For $\phi = 0.5\%$, the volume decreases by approximately 7% to 12% compared to the case with the base fluid, depending on the coolant Reynolds number. This result confirms that even moderate improvements in the overall coefficient can translate into significant reductions in the total volume of the equipment, particularly in compact heat exchangers where the specific area is high and small variations in U directly impact the required size.

However, the use of nanofluids introduces hydraulic penalties, mainly on the coolant side. Figure 14 shows the coolant pressure drop for different concentrations, where a systematic increase is observed as ϕ increases. Quantitatively, the pressure drop increases by approximately 8% to 15% when going from ϕ=0 to ϕ=0.5%. This increase is associated with the increase in the effective viscosity of the nanofluid, which increases the friction factor and friction losses in the heat exchanger channels. This result is particularly important from the point of view of pumping power, since moderate increases in ΔP can translate into an increase in energy consumption in the cooling circuit, especially if the system operates continuously.

In industrial applications, this effect represents the main limiting factor for the adoption of nanofluids: although thermal intensification is achieved, the increase in pressure losses can reduce or even negate the overall benefit when the total energy consumption of the system is evaluated. Therefore, the selection of the optimal concentration should not be based solely on maximizing

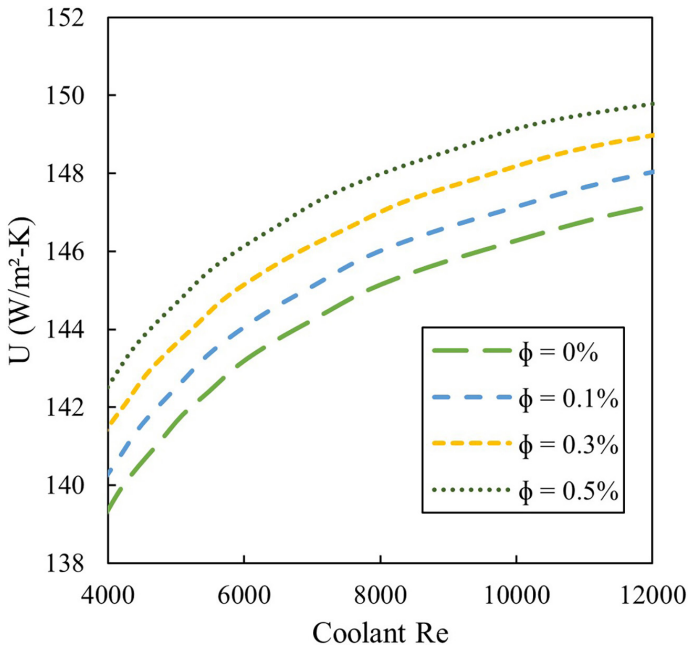

Figure 12. Overall heat transfer coefficient evaluated at different nanofluid concentrations for $Re_g = 8000$, for a range of 4000 to 12000 of the coolant Reynolds number

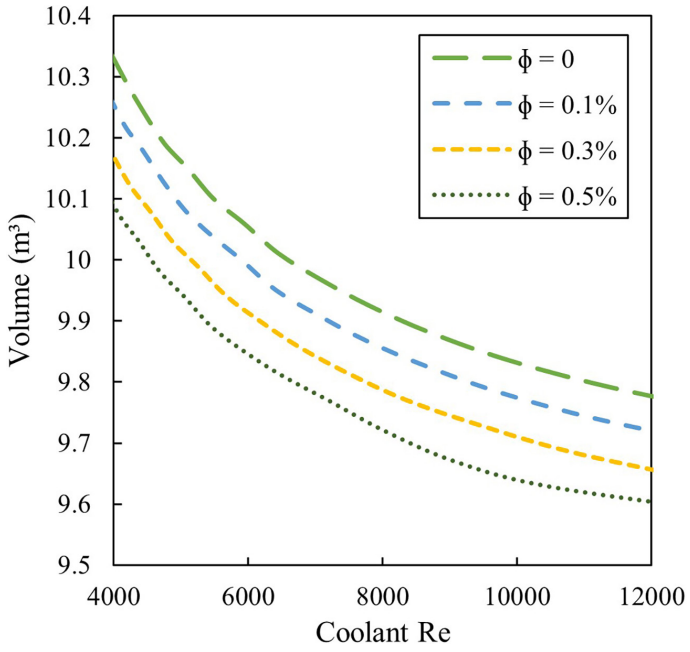

Figure 13. Intercooler volume evaluated at different nanofluid concentrations for Re_g = 8000, for a range of 4000 to 12000 of the coolant Reynolds number

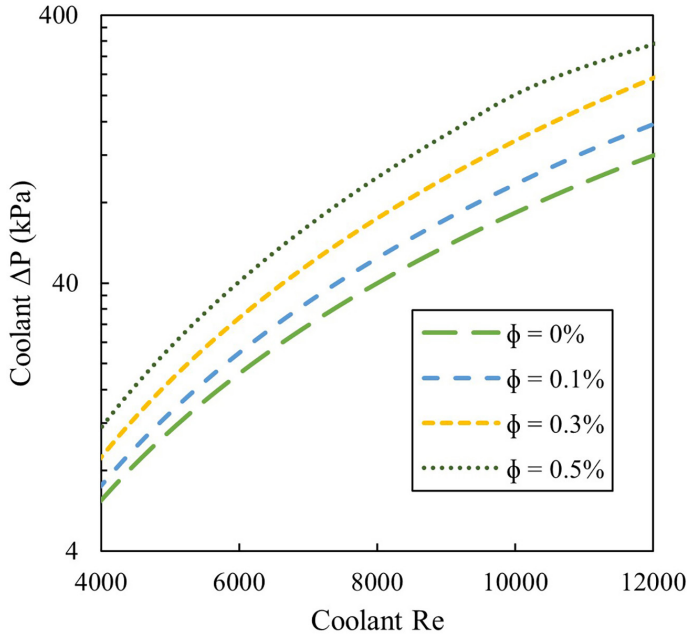

Figure 14. Pressure drop on the coolant side evaluated at different nanofluid concentrations for Re_g = 8000, for a range of 4000 to 12000 of the coolant Reynolds number

U, but on achieving a balance between thermal improvement and hydraulic penalty.

Figure 15 shows the pressure drop on the gas side for different concentrations. Unlike the coolant, the influence of ϕ on the gas pressure drop is indirect and moderate, with variations of less than 5–7%. This indicates that the effect of the nanofluid does not significantly alter the hydrodynamic behavior of the gas, since this is dominated by the geometry of the heat exchanger and the fixed gas Reynolds number. This result is favorable, given that in compression stations the dominant energy cost is usually associated with gas compression, not coolant pumping. Consequently, the use of nanofluids in the coolant does not critically increase the gas-side penalty.

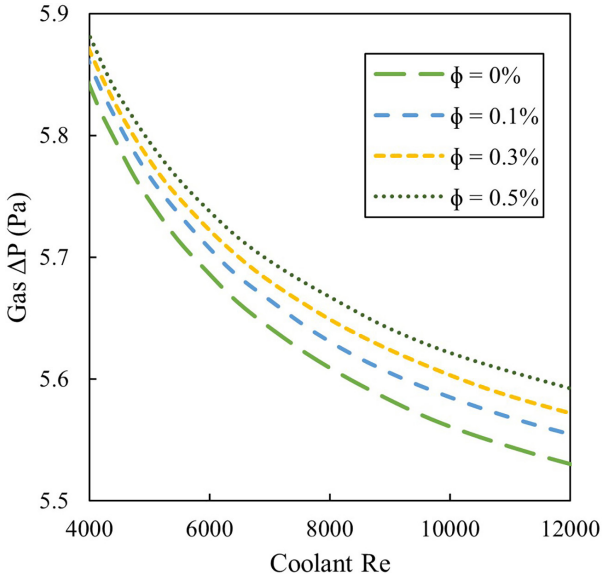

Figure 15. Gas-side pressure drop evaluated at different nanofluid concentrations for Re_g = 8000, for a range of 4000 to 12000 of the coolant Reynolds number

Overall, the results indicate that the use of CuO–water nanofluids constitutes a viable strategy for enhancing intercooler thermal performance and reducing exchanger size, particularly when system compactness is a primary design objective. The observed improvement in overall heat transfer coefficient and the associated volume reduction fall within the range commonly reported in the literature for low nanoparticle volume fractions under turbulent flow conditions. Previous studies have similarly identified moderate thermal enhancement accompanied by increased pressure drop due to higher effective viscosity. However, unlike investigations conducted in simplified channel geometries or laboratory-scale systems, the present analysis evaluates nanofluid performance within a compact plate-fin configuration under realistic natural gas compression conditions, thereby extending existing findings to a more application-oriented framework. Within the analyzed range, moderate concentrations ($\phi \approx 0.3$–0.5%) provide an attractive compromise between volume reduction (≈ 7–12%) and increase in coolant pressure drop (≈ 8–15%), suggesting that industrial implementation is feasible provided that cooling circuit operation and pumping power requirements are properly optimized.

CONCLUSIONS

In this work, a numerical model was developed to evaluate the thermo-hydraulic performance of a compact plate-fin intercooler applied to a natural gas compression station, considering the influence of gas Reynolds number, imposed coolant temperature difference, and the use of CuO–water nanofluids. The results confirm trends widely reported for compact heat exchangers, namely that increasing Reynolds number enhances convective heat transfer while increasing frictional losses; however, the present study extends previous findings by quantifying these effects simultaneously in terms of overall heat transfer coefficient, exchanger volume, and pressure drop under realistic natural gas compression conditions.

The gas Reynolds number was identified as the dominant parameter, increasing the overall heat transfer coefficient by approximately 35–40% and reducing the required exchanger volume by up to 30–45% when increased from 4000 to 12000, albeit with a 250–350% rise in gas-side pressure drop. Nevertheless, the absolute magnitude of this pressure drop remains very small (approximately 2–18 Pa), which represents a negligible fraction of the operating pressure of the compression system. Increasing the temperature difference (ΔT = 8–12 °C) had a limited effect on U (2–4%) but enabled an 8–12% reduction in exchanger volume without significant hydraulic penalties. The incorporation of CuO–water nanofluids ($\phi \leq 0.5\%$) improved U by 6–9% and reduced volume by up to 7–12%, although coolant pressure drop increased by 8–15% due to higher effective viscosity. The reported gas-side pressure drops correspond to channel-level frictional losses and may underestimate total

system pressure losses in practical installations where header and distribution effects are present.

From a practical perspective, these findings provide a structured thermo-hydraulic trade-off framework for the design and optimization of compact intercoolers in natural gas compression systems. Nevertheless, the present study is limited to steady-state numerical modeling using established correlations and does not include experimental validation or long-term operational considerations. Future research should focus on experimental verification under industrial conditions, transient operation analysis, assessment of long-term nanofluid stability and fouling effects, and multi-objective optimization incorporating economic and energy consumption criteria.

REFERENCES

1. Ojo O.B., Hegab A., Pilidis P. Impact of compressor station availability on the techno-economics of natural gas pipeline transportation. Energies 2025; 18: 4243. https://doi.org/10.3390/en18164243
2. Shoghl S.N., Pazuki G. Compressor/pump stations in natural gas transmission pipelines. Advances in Natural Gas: Formation, Processing, and Applications Volume 6: Natural Gas Transportation and Storage 2024; 177–236. https://doi.org/10.1016/b978-0-443-19225-8.00006-8
3. Lugo-Méndez H., Lopez-Arenas T., Torres-Aldaco A., Torres-González E.V., Sales-Cruz M., Lugo-Leyte R.. Interstage pressures of a multistage compressor with intercooling. Entropy 2021; 23: 351. https://doi.org/10.3390/e23030351
4. Dolbec A.C., Cohn A. Gas-turbine power plants. Encyclopedia of Physical Science and Technology 2003:487–500. https://doi.org/10.1016/b0-12-227410-5/00277-5
5. Yu C., Zhang W., Xue X., Lou J., Lao G.. Analysis of water-cooled intercooler thermal characteristics. Energies 2021; 14: 8332. https://doi.org/10.3390/en14248332
6. Zhao N., Wen X., Li S. An evaluation of the application of nanofluids in intercooled cycle marine gas turbine intercooler. Journal of Engineering for Gas Turbines and Power 2015; 138. https://doi.org/10.1115/1.4031170
7. Almertejy A., Rashid M.M., Ali N., Almurtaji S. Application of nanofluids in gas turbine and intercoolers—A comprehensive review. Nanomaterials 2022; 12: 338. https://doi.org/10.3390/nano12030338
8. Gupta M., Singh V., Kumar R., Said Z. A review on thermophysical properties of nanofluids and heat transfer applications. Renewable and Sustainable Energy Reviews 2017; 74: 638–70. https://doi.org/10.1016/j.rser.2017.02.073
9. Rahman M.A., Hasnain S.M.M., Pandey S., Tapalova A., Akylbekov N., Zairov R. Review on nanofluids: Preparation, properties, stability, and thermal performance augmentation in heat transfer applications. ACS Omega 2024. https://doi.org/10.1021/acsomega.4c03279
10. Bizuneh Y.E., Kassie T.D., Gebresilassie E.B., Bizuneh A.E. Numerical investigation on heat transfer of CuO-water nano-fluid in a circular pipe with twisted tape inserts. International Journal of Thermofluids 2025; 27: 101260. https://doi.org/10.1016/j.ijft.2025.101260
11. Lavanya B., Srinivas G., Babu B.S., Makinde O.D. Numerical analysis of heat transfer of CuO-water nanofluid through a square channel with heated inner triangular groove. Archives of Thermodynamics 2025: 83–83. https://doi.org/10.24425/ather.2025.154183
12. Jayanthi N., Venkatesh M., Suresh K. R., Ramesh B. S., Prabakar P. Experimental evaluation of CuO and Al_2O_3 nanofluids for enhanced heat transfer in evacuated tube heat pipe solar collectors. Results in Engineering 2025; 27: 106299. https://doi.org/10.1016/j.rineng.2025.106299
13. Abdelmagied M. Numerical analysis on heat transfer enhancement of Al_2O_3 and CuO-water nanofluids in annular curved tubes. Int J Air-Cond Ref 2025; 33. https://doi.org/10.1007/s44189-024-00066-8
14. Khatoon S., Ishaque S., Kim M.-H. Modeling and analysis of air-cooled heat exchanger integrated with supercritical carbon dioxide recompression Brayton cycle. Energy Conversion and Management 2021; 232: 113895. https://doi.org/10.1016/j.enconman.2021.113895
15. Nimbal S. S., Nalawade M. K. Design and analysis of multi-stage intercooler. IJITEE 2019; 8: 1705–10. https://doi.org/10.35940/ijitee.j9021.0881019
16. Almurtaji S., Ali N., Teixeira J.A., Addali A. Effect of multi-walled carbon nanotubes-based nanofluids on marine gas turbine intercooler performance. Nanomaterials 2021; 11: 2300. https://doi.org/10.3390/nano11092300
17. Mezrakchi R.A. Investigation of various hybrid nanofluids to enhance the performance of a shell and tube heat exchanger. AIMSE 2024; 12: 235–55. https://doi.org/10.3934/energy.2024011
18. Chintala V., Vikesh S., Karn A. Efficiency and effectiveness enhancement of an intercooler of two-stage air compressor by low-cost Al_2O_3/water nanofluids. Heat Trans 2020; 49: 2577–94. https://doi.org/10.1002/htj.21735
19. Canazas J., Kamyshnikov O. Heat transfer and pressure drop performance of a hydraulic mining shovel radiator by using ethylene glycol/water-based Al_2O_3 Nanofluids. IJHT 2022; 40: 273–81. https://doi.org/10.18280/ijht.400132

20. Şahin M., Öztürk M. CFD analysis of the characteristic of a heat exchanger with counter flow shell tube under biogas-nanofluid conditions. J Therm Anal Calorim 2025; 150: 9413–22. https://doi.org/10.1007/s10973-025-14276-8
21. Ríos-Mercado R.Z., Borraz-Sánchez C. Optimization problems in natural gas transportation systems: A state-of-the-art review. Applied Energy 2015; 147: 536–55. https://doi.org/10.1016/j.apenergy.2015.03.017
22. Yilmazoglu M.Z., Amirabedin E., Shotorban B. Waste heat utilization in natural gas pipeline compression stations by an organic Rankine cycle. Energy Exploration & Exploitation 2014; 32: 317–28. https://doi.org/10.1260/0144-5987.32.2.317
23. Ghilardi L.M.P., Naik S., Biegler L.T., Casella F., Palazzo R., Martelli E. Optimal operation of gas transport pipelines with detailed MILP and NLP models. Ind Eng Chem Res 2025; 64: 14560–75. https://doi.org/10.1021/acs.iecr.5c01043
24. Saha S.K., Ranjan H., Emani M.S., Bharti A.K. Heat transfer enhancement in plate and fin extended surfaces. Springer International Publishing; 2020. https://doi.org/10.1007/978-3-030-20736-6
25. Canazas J. Field study on the air-side heat transfer performance of copper finned-flat tubes for heavy-duty truck radiators. IJHT 2021; 39: 1451–9. https://doi.org/10.18280/ijht.390506
26. Kays, W.M., London, A.L. Compact Heat Exchangers. KriegerPub. Co., Malabar, FL, USA; 1998.
27. Pachpute S.L., More K.C. Design optimization of a plate-fin heat exchanger with metaheuristic hybrid algorithm. Heat Trans 2024; 54: 1163–72. https://doi.org/10.1002/htj.23213
28. Vajjha R.S., Das D.K., Kulkarni D.P. Development of new correlations for convective heat transfer and friction factor in turbulent regime for nanofluids. International Journal of Heat and Mass Transfer 2010; 53: 4607–18. https://doi.org/10.1016/j.ijheatmasstransfer.2010.06.032
29. Gnielinski V. On heat transfer in tubes. International Journal of Heat and Mass Transfer 2013; 63: 134–40. https://doi.org/10.1016/j.ijheatmasstransfer.2013.04.015
30. Jia W., Song S., Zhang L., Wang C., Krivosheyev P., Chen D., et al. Ignition delay time and methane time history in hydrogen-natural gas surrogate blends: A shock tube study. Combustion and Flame 2025; 277: 114191. https://doi.org/10.1016/j.combustflame.2025.114191
31. Shirizadeh B., Villavicencio M., Douguet S., Trüby J., Bou I. C., Seck G.S., et al. The impact of methane leakage on the role of natural gas in the European energy transition. Nat Commun 2023; 14. https://doi.org/10.1038/s41467-023-41527-9
32. Hanley H.J.M., Haynes W.M., McCarty R.D. The viscosity and thermal conductivity coefficients for dense gaseous and liquid methane. Journal of Physical and Chemical Reference Data 1977; 6: 597–610. https://doi.org/10.1063/1.555553
33. Prasad R.C., Mani N., Venart J.E.S. Thermal conductivity of methane. Int J Thermophys 1984; 5: 265–79. https://doi.org/10.1007/bf00507836
34. Ewing M.B., Goodwin A.R.H. Speeds of sound, perfect-gas heat capacities, and acoustic virial coefficients for methane determined using a spherical resonator at temperatures between 255 K and 300 K and pressures in the range 171 kPa to 7.1 MPa. The Journal of Chemical Thermodynamics 1992; 24: 1257–74. https://doi.org/10.1016/s0021-9614(05)80266-6
35. Wagner W., Pruß A. The IAPWS Formulation 1995 for the thermodynamic properties of ordinary water substance for general and scientific use. Journal of Physical and Chemical Reference Data 2002; 31: 387–535. https://doi.org/10.1063/1.1461829
36. Huber M.L., Perkins R.A., Laesecke A., Friend D.G., Sengers J.V., Assael M.J., et al. New international formulation for the viscosity of H_2O. Journal of Physical and Chemical Reference Data 2009; 38: 101–25. https://doi.org/10.1063/1.3088050
37. Huber M.L., Perkins R.A., Friend D.G., Sengers J.V., Assael M.J., Metaxa I.N., et al. New international formulation for the thermal conductivity of H_2O. Journal of Physical and Chemical Reference Data 2012; 41. https://doi.org/10.1063/1.4738955
38. Yadav D., Sanserwal M. A comprehensive review of the effects of various factors on the thermal conductivity and rheological characteristics of CNT nanofluids. J Therm Anal Calorim 2022; 148: 1723–63. https://doi.org/10.1007/s10973-022-11821-7
39. Ghazwani M., Hani U. To study the thermodynamic properties of magnetic field on water based CoFe2O4 nanofluids. Sci Rep 2025; 15. https://doi.org/10.1038/s41598-025-89265-w
40. Pak B.C., Cho Y.I. Hydrodynamic and heat transfer study of dispersed fluids with submicron metallic oxide particles. Experimental Heat Transfer 1998; 11: 151–70. https://doi.org/10.1080/08916159808946559
41. Xuan Y., Li Q. Heat transfer enhancement of nanofluids. International Journal of Heat and Fluid Flow 2000; 21: 58–64. https://doi.org/10.1016/s0142-727x(99)00067-3
42. Kondakrindi K. R., Reddigari M. R., Konireddy H. R., Maheswari U. C. Nanofluids (CuO & TiO_2) - water as heat transfer fluid in a thermal energy storage system for applications of solar heating: An experimental study. Therm Sci 2023; 27: 4375–88. https://doi.org/10.2298/tsci221215080k
43. Girhe N.B., Botewad S.N., More C.V., Kadam S.B., Pawar P.P., Kadam A.B. Development of water-based CuO, TiO_2 and ZnO nanofluids and comparative study of thermal conductivity and viscosity. Pramana - J Phys 2023; 97. https://doi.org/10.1007/s12043-023-02546-9